Journal of Energy Technology

JET Volume 14 (2021) p.p. 41-58
Issue 4, December 2021
Type of article 1.01
www.fe.um.si/en/jet.html

DESIGNING AN ELECTROMECHANICAL GENERATOR FOR ENERGY HARVESTING

NAČRTOVANJE ELEKTROMEHANSKEGA GENERATORJA ZA IZRABO ENERGIJE GIBANJA

Franjo Pranjić[R], Nejc Smolar[1], Peter Virtič[1]

Keywords: energy harvest, linear generator, permanent magnets, Finite Element Method

Abstract

Five different designs of tubular electromechanical generator for low frequency energy harvesting have been investigated in this paper. In order to design a simple and robust generator, models were constructed out of permanent magnets, steel and windings. In all five generator models, round movers were used in spherical and cylindrical form- for four models solely permanent magnets were used, and in one model, there was steel present in the mover. The movers are slid or rolled through a tube, and induce voltage in the stator winding. All windings were constructed with the same cross-section dimensions and number of turns. To compare different models, 3D analysis with the Finite Element Method was performed, in order to determine the magnetic flux through the windings. The induced voltage was calculated using the results of the analysis. As a result of the different winding geometries, the average turn length varied for the different designs, subsequently altering resistance and inductance, which affected the generator`s power output and losses. To simulate the generator`s dynamics, an equivalent circuit model was constructed using the Simulink software and data obtained previously from a 3D electromagnetic analysis. With the Simulink model, we coupled the mechanical and electrical systems together to acquire the harvester yields.

[R] Corresponding author: Franjo Pranjić, University of Maribor, Faculty of Energy Technology, Hočevarjev trg 1, 8270 Krško, Slovenija, Email: franjo.pranjic@um.si

[1] University of Maribor, Faculty of Energy Technology

Povzetek

V članku je predstavljenih 5 različnih izvedb cevnega nizkofrekvenčnega elektromehanskega generatorja za izrabo energije gibanja. Z namenom oblikovanja preprostega in robustnega generatorja so modeli sestavljeni iz trajnih magnetov, jekla in navitij. Pri vseh modelih generatorjev sta za okrogli gibljivi del uporabljeni sferična in cilindrična oblika - pri štirih modelih so uporabljeni izključno trajni magneti, pri enem pa je prisotno jeklo. Gibljivi del drsi ali pa se valja skozi cev in pri tem inducira napetost v navitju statorja. Pri vsakem modelu imajo navitja enak presek ter enako število ovojev. Za primerjavo različnih modelov je bila izvedena 3D-analiza z uporabo metode končnih elementov za določitev magnetnega pretoka skozi navitja, na podlagi katerih je izračunana inducirana napetost. Zaradi različnih geometrij navitij se je povprečna dolžina ovoja pri različnih izvedbah spreminjala, kar je posledično spreminjalo upornost in induktivnost ter s tem vplivalo na izhodno moč in izgube generatorja. Za simulacijo dinamike generatorjev je bilo z uporabo programa Simulink in predhodno pridobljenih podatkov iz 3D-elektromagnetne analize določeno nadomestno vezje modela. Za določanje izplena smo z modelom v programu Simulink združili mehanske in električne sisteme.

1 INTRODUCTION

World energy demand is constantly on the rise and, at the same time, there is an urgent demand/need to decarbonise energy production and substitute it with renewable energy. This goal could be achieved easily with the conversion of sea energy, which could replace all current electrical power production [1]. Even though there are 153 coastal countries, only a small amount of energy is currently utilised using sea harvesting, which could capitalise this abundant renewable energy source.

In recent years a lot of research has been done in the field of Sea wave energy exploitation. Different models were developed for energy harvesting, from using piezoelectric, rotational to linear generators, in order to supply grids with renewable energy [2]-[3]. Part of the research has focused on generating power for self-sustainable systems. Sea wave energy harvesting anchored buoys are one of them, where linear generators are used mostly [4]–[7], since they offer high energy density. As diverse as these sea harvesting methods may be, all of them require a fixed anchorage. However, some mobile offshore applications also demand a constant power supply, and with no option to be connected to the power grid, the need arises for self-sustaining systems. Since PV panels are one of more popular choices for self-sustaining applications, due to the abundance of solar energy, such systems are not always the optimal choice, especially as solar powered systems have a big disadvantage in cloudy and foggy conditions and at high latitudes, where daily solar energy during winters is very low. A second problem occurs for cases where the demand for energy is mostly at night time, where expensive energy storages have to be integrated. To minimise energy storage, or even eliminate it, many micro generators have been developed for non-stationary methods of harvesting, normally utilising vibrations or human motions [8]–[15].

The purpose of this article is to create a simple, durable and cost efficient design of a mobile harvester that can generate sufficient electrical energy on the move. The proposed designs of the harvester are constructed only out of a stator, a mover and semiconductors to transform alternating power into direct power .

The stator structure is coreless, which means that there is no iron present. Multiple phase windings are wound on a plastic tube, through which the mover displaces. Two different methods of mover displacement have been used, namely translational, where the friction was minimised by wheels, and rolling motion in the second case, where the mover was rolling on it's outer surface or the surface of the spindles, inducing voltage into the surrounding windings.

A detailed geometrical description of the models, input data, calculation methods, as well geometry analysis with the Finite Element Method is presented in the first part of the article. In the second part, the results of the AC induced voltages at the winding terminals and DC link are presented, and, finally, with help of Simulink simulations, an analysis of the power generation of the harvester coupled with a mechanical model at different loads. Calculations of electrical efficiency and the yield of available energy are performed and the results are compared and discussed.

2 MODELS

The presented sea wave energy harvesters can be divided into two parts. A generating and converting part, where the generating part transforms mechanical energy from the moving part (mover) into electrical energy according to Faraday's law of induction, and the converting part, assembled from semiconductor diodes that convert the alternating voltage to a direct one.

The generating part consists of stationary windings (stator) and a mover, as Fig.1 shows.

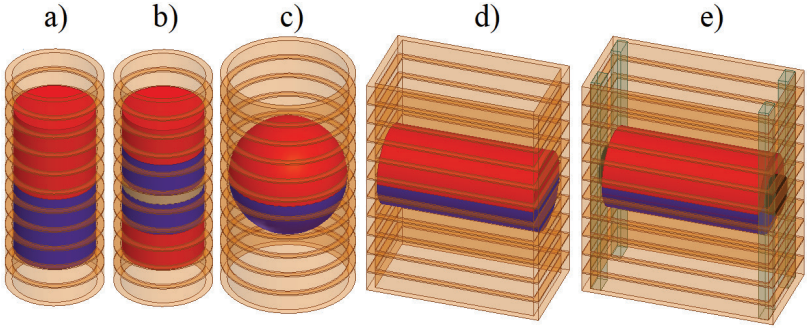

Figure 1: *Energy harvester designs:*
a) Model A - translational cylindrical solid PM mover; b) Model B - translational cylindrical mover with two identical PMs and inserted steel plate in between; c) Model C - rolling spherical mover with solid PM; d) Model D - rolling cylindrical solid PM mover; e) Model E - rolling cylindrical solid PM mover with spindles

Models A and B utilise the translational movement of the cylindrical movers to displace through the stator. Spherical mover C and cylindrical movers D and E use a rolling motion to displace through the stator. The Model C and D movers are rolling on the mover's circumference, and model E's mover is rolling on the circumference of the added spindles, which have been placed on each side concentric to the mover's axis. The basic idea of spindles is to increase the mover's rotational speed in order to increase the magnetic flux change rate.

Movers A, C, D and E are made of single solid two-pole permanent magnets (PM), presented with the red and blue colours in Fig. 1. Model B was assembled from two identical PMs,

between which a steel disc (grey colour in Fig. 1b) was inserted and glued to the PMs. The PMs` magnetisation vectors were facing each other, while the steel disc concentrated the magnetic field to a smaller area, as suggested in [16, 17]. In such an assembly, the mover has three magnetic poles, compared to two poles in the other movers.

A sintered neodymium iron boron (NdFeB) N40 magnet with 1.28 T remanence and -895 kA/m coercivity were used for the PMs` characteristics. The magnets magnetisation vectors were oriented in the displacing direction of the mover, aligned with the coordinate systems Z axis (Fig. 2). The rolling mover's magnetisation vector was, therefore, perpendicular to the mover's rotational axis plane, and was rotating in the XZ plane and displacing along the Z-axis, as sliding movers do.

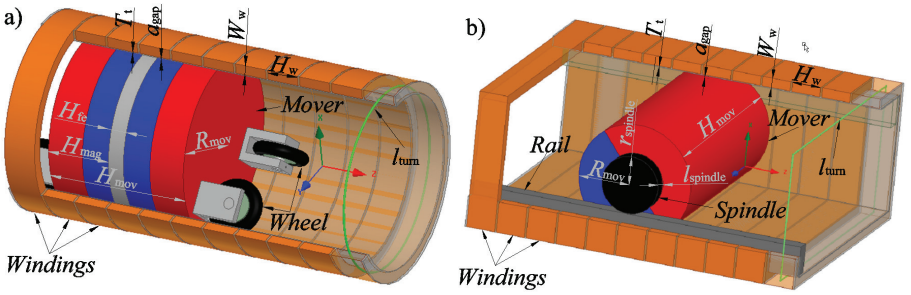

Figure 2: *Schematic harvester/generator structure: a) Model B, b) Model E*

The mass of the movers is identical in all models, 20 kg. This means that, in cases of movers with a single piece PM, the magnet weight is the full 20 kg, and in the case of an assembled mover (model B) each magnet weighed 8.88 kg and the steel plate took up the rest of the mass towards 20 kg, as presented in Table 1.

Table 1: *Harvester designs` parameters*

Symbol	Model				
	A	B	C	D	E
	MOVER				
Mass of the mover m_{mov} (kg)	20	20	20	20	20
Density of the permanent magnet and steel $\rho_{NdFeB} = \rho_{Fe}$ (kg/m^3)	7400	7400	7400	7400	7400
Volume of the mover V_{mov} (cm^3)	2702,7	2702,7	2702,7	2702,7	2702,7
Radius of the mover R_{mov} (mm)	80	80	86,41	50	50
Height of the mover H_{mov} (mm)	134,42	134,42	-	344,12	344,12
Height of the permanent magnet h_{mag} (mm)	134,42	66,09	-	344,12	344,12
Mass of the permanent magnet m_{mag} (kg)	20	2x 8,88	20	20	20

To be continued

Continuation

Height of the steel h_{fe} (mm)	-	15	-	-	-
Mass of the steel m_{fe} (kg)	-	2,23	-	-	-
Length of the spindle $l_{spindle}$ (mm)	-	-	-	-	15
Radius of the spindle $r_{spindle}$ (mm)	-	-	-	-	30
	WINDINGS				
Air gap a_{gap} (mm)	1	1	1	1	1
Tube thickness T_t (mm)	1	1	1	1	1
Height of the winding H_w (mm)	30	30	30	30	30
Width of the winding W_w (mm)	10	10	10	10	10
Filling factor FF	0,6	0,6	0,6	0,6	0,6
Number of turns in one winding N_{turn}	100	100	100	100	100
Length of an average turn l_{turn} (mm)	546,64	546,64	586,92	904,24	964,24
Winding resistance R_w (Ω)	0,51	0,51	0,55	0,84	0,9
Winding inductance L_w (mH)	2,4	2,4	2,64	3,89	4,12

We did not take in to account the mass of the wheels and spindles, which were made of plastic, as they would increase total mass of the movers by less than 1 %. The cylinder`s height was calculated from the defined radius of the movers and the mass of 20 kg, where the same mass density of 7400 kg/m3 was used for the PM and the steel.

We enclosed the movers with a 1 mm thick PVC tube, which provided structural hardness and served as a winding base for the windings. To ensure even spacing for unobstructed movement, a 1 mm air gap was left between the tube and the mover. The general shape of the windings was therefore imposed by the shape of the mover, as shown in Fig. 1. To maximise the magnetic flux, the windings were placed perpendicular to the movement direction in the XY – plane, as shown in Fig. 2. The windings were made of copper wires with 100 turns (Nturn), which were wound concentrically. In the case of model E (the cylindrical mover with spindles) we additionally spread the winding in the Y axis direction to make space for spindles, and rails on which the spindles would roll. The spindles and rails were also made of plastic so as not to disturb th magnetic field or to make any losses due to eddy currents. All windings had the same rectangular cross-section area of 300 mm2, with 30 mm height of the winding (Hw) (Z axis) and 10 mm thickness (Ww). For further calculations, we took a filling factor of 0.6, due to the uncomplicated and simple winding geometry. The windings were spaced 2 mm apart, to leave space for the plastic separation walls, to divide the phases.

To establish equal conditions, all the movers had the same initial kinetic energy, determined by the potential energy of 0.5 m elevation difference (*H*). We made a presumption that movement in simulations was frictionless, as minimal rolling resistance and low velocities would amount in real conditions to tiny mechanical energy losses.

With this simplification, we could determine the initial velocity of movers A and B, using the simple equation for free falling objects, $v=(g\cdot H)^{0,5}$. For the rolling movers` translational velocities Eq (1) had to be used, where $I$ presents the movers` inertia and m_{mov} presented the mass of mover. In the case of the rolling movers, the radius of the circumferential surface on which mover rolled was presented with the value r_{base}.

$$v = \sqrt{\frac{2 \cdot m_{mov} gH}{m_{mov} + \frac{I}{r_{base}^2}}} \tag{2.1}$$

3 MAGNETIC FLUX AND INDUCED VOLTAGE

An analysis of the magnetic flux through the windings as themover displaced, was performed with 2 mm displacement steps, where the mover displaced by 1.2 m through the tube. All 17 windings were placed onto the tube, which gave 542 mm of total windings` width. The centre of the mass of the ninth winding was placed into the coordinate system centre, so equal amounts of windings were laying on both sides of the coordinate system.

The generator`s geometry was then analysed with ANSYS Maxwell using the 3D magnetostatic Finite Element Method, in order to obtain the magnetic flux and inductivity of the windings. In the case of model B we also checked that the magnetic field density in the steel plate did not reach the saturation point of 1.8 T.

Figs. 3 a) and b) are showing the magnetic flux waveforms of the translational movers. When the mover approaches the observed winding the magnetic flux starts to rise, as a result of more magnetic field lines looping through the winding. When both the mover's and windings' centres of mass were aligned the Dipole PM mover's magnetic flux reached the maximum. In the case of the three pole mover, the magnetic flux reached the maximum when the PM's centre of mass crossed the windings' centre plane, and the magnetic flux dropped rapidly back to zero when the mover's centre of mass reached the windings` centre plane, and changed polarity, due to the opposite magnetisation of the adjacent magnet. From models A and B magnetic flux waveforms, we can see that the waveforms are identical in amplitude and shape, but shifted along the Z axis by the winding's centre of mass distance, which is equal to the sum of the winding's height and the air gap between them.

As we can see from Figs. 3 c), d) and e), the rolling mover's magnetic flux waveforms are more complex. We can view them as a superposition of two motions through winding. The first one is translational and the second one is rotational, where the angle of the constant magnetic field changes relative to the winding's plane as the mover rolls through the tube. Therefore, the magnetic flux changes with the cosine function, where the magnetic flux reaches its highest value when the magnetic field vector aligns with the winding's normal plane, and goes through zero when the magnetic field vector is parallel with the winding`s plane. As a result, the magnetic flux through the windings reaches its maximum and minimum in one full rotation and goes through zero between the extremes every half rotation. Combining the effects of proximity and rotating magnetisation angle, we obtained the displayed magnetic flux waveforms. Comparing Figs. 3 d) and e), we can see that the spindles indeed increased the magnetic flux change rate, as the mover E was forced in to a higher angular velocity, and, therefore, made more revolutions in one pass through the windings.

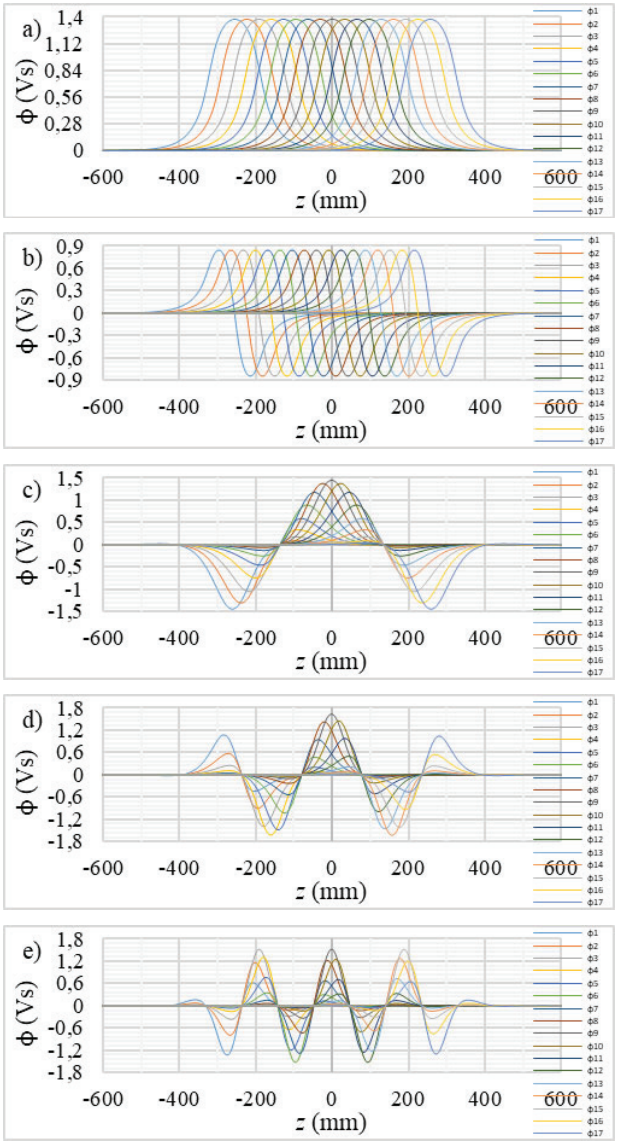

Figure 3: Magnetic flux waveforms: a) Model A, b) Model B, c) Model C, d) Model D, e) Model E

With the defined magnetic flux waveforms for different models we implemented Faraday – Lenz's law of electromagnetic induction e(t)=-dϕ/dt, to calculate the induced voltages in the windings. From the equation for electromagnetic induction we derived Eq (2), which gives the induced voltage in between two positions of the mover's centre of mass at a defined constant velocity. [6]

$$e\left(z_{\mathrm{i}}+\frac{z_{\mathrm{i+1}}-z_{\mathrm{i}}}{2}\right)=-\frac{\left(\varphi\left(z_{\mathrm{i+1}}\right)-\varphi\left(z_{\mathrm{i}}\right)\right)\cdot v}{z_{\mathrm{i+1}}-z_{\mathrm{i}}} \tag{3.1}$$

From the magnetic flux waveforms, using initial velocity, we calculated the induced voltages for the individual windings, to obtain the voltage waveforms, as shown in Fig. 4. To compare the output voltages, we first needed to convert them to direct voltages, with the use of semiconductors arranged in a Greatz bridge.

As result of the different amplitudes of the induced voltages in the windings at the same position of the mover, only the pair of windings with the highest and lowest amplitude would contribute to the voltage output. As the mover progressed through the windings the induced voltages would cross, and the next winding would generate a higher induced voltage and become active.

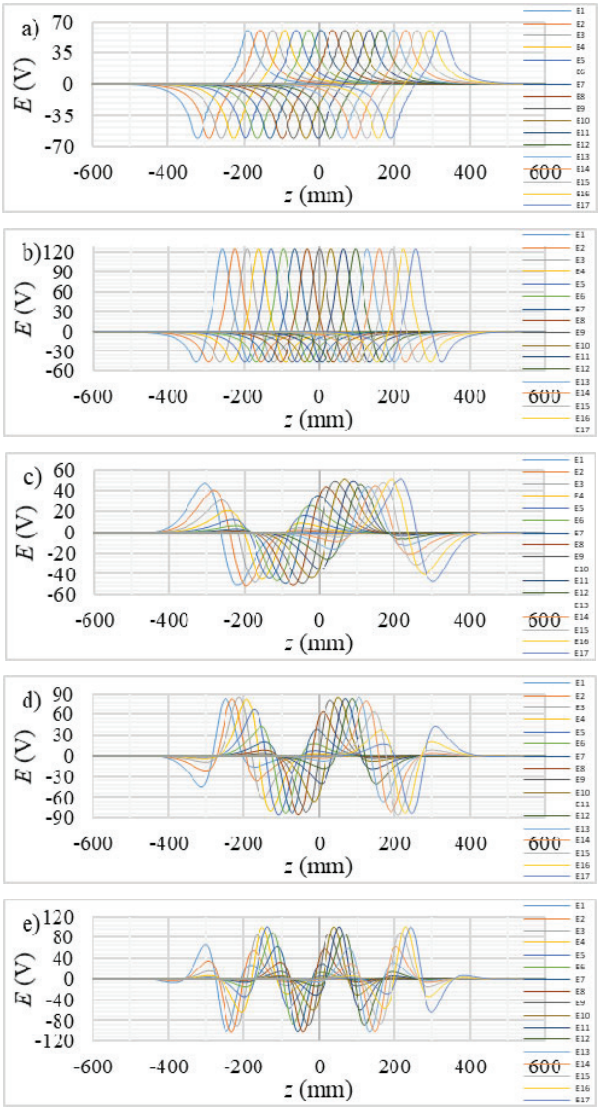

Figure 4: *Induced voltage the waveforms at a constant velocity with the windings wound in the same direction: a) Model A, b) Model B, c) Model C, d) Model D, e) Model E*

Therefore, for transformation into direct voltage at an open circuit, we took the positive and negative extremes at all positions and combined them into positive and negative lines, orange and blue lines as shown in Fig. 5. To get the total potential difference between the positive and negative voltages, we summed the absolute values together, shown by the grey line in Fig. 5.

From the potential difference we calculated the RMS values with Eq 3, to compare the induced voltages for all models on the DC side, in a range from -499 mm to 499 mm,

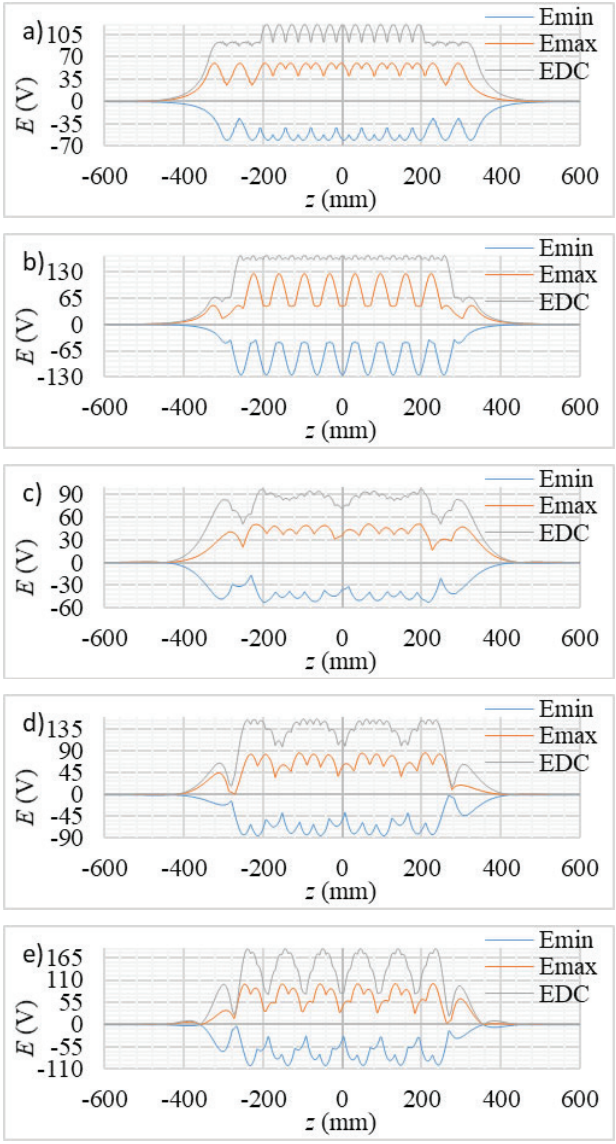

Figure 5: *Direct open circuit voltage at a constant velocity with the windings wound in alternating directions: a) Model A, b) Model B, c) Model C, d) Model D, e) Model E*

$$E_{\text{rms}} = \sqrt{\frac{1}{N}\sum_{\text{n}}(E_{\text{DC}})^2(n)} \tag{3.2}$$

with the translational movers A and B. The design with three poles B scored the highest with 119.48 V, due to the narrow middle pole with a high magnetic flux density. Model A had the second highest RMS voltage of 81.43 V. The rolling cylindrical designs` outputs ranked in the middle, with 69.18 V for model D and 67.04 V for model E. The spherical model had the lowest induced DC voltage of 45.99 V

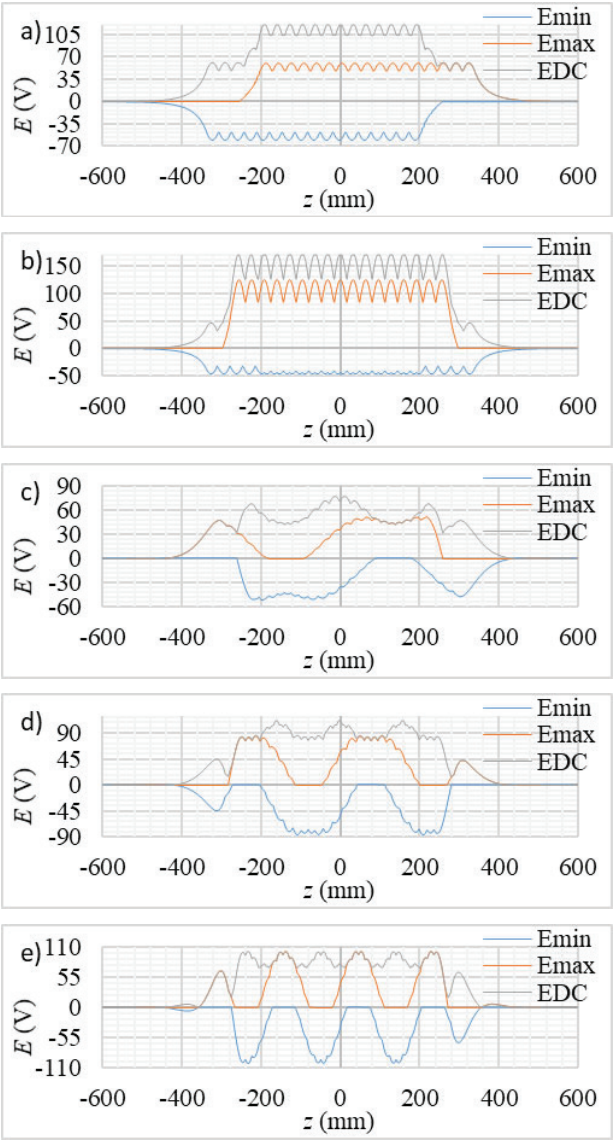

Figure 6: *Direct voltage open circuit at a constant velocity with the windings wound in the same direction: a) Model A, b) Model B, c) Model C, d) Model D, e) Model E*

To create a higher voltage difference on the DC side, the windings were wound alternatingly (Fig. 6) in all models, and the RMS values were recalculated. As the results showed RMS values improved up to 41 % with such windings` configuration, models B, C and E also had smoother induced voltages.

With alternatingly wound windings, the highest improvement was made with the rolling models. The sphere model voltage improved by 25.56 %, resulting in 61.78 V. The second highest improvement was made on D, increasing the RMS induced voltage by 35.55 V, going up to 104.72 V.

The highest improvement on RMS voltage output was made by the cylindrical mover model with spindles, where the voltage increased from 67.04 to 113.49 V. The model with the 3 pole translational mover also improved by about 6.44 %, and still had highest induced voltage on the DC side.

4 SIMULINK MODEL

To research the harvester's operation, we created in Simulink Simscape an equivalent circuit model for the harvester. Each winding was modelled with a resistor, inductor and controlled voltage source. Resistance was determined with the calculated value from the average wire loop length, filling factor and number of turns. Inductance for the windings was obtained from ANSYS, as presented in Table 1.

From the magnetic flux waveforms, the magnetic flux gradients were calculated along z positions, which were used to link the discrete magnetic flux data to the voltage sources. We used dynamic lookup tables, which gave magnetic flux gradients for every 2 mm section. The magnetic flux gradients were then multiplied with the velocity in order to obtain the induced voltages, which were implemented in the circuit with the voltage controlled source. An identical winding circuit was used for all 17 windings with a matching winding magnetic flux gradient, as is shown in Fig. 7.

Figure 7: Direct voltage

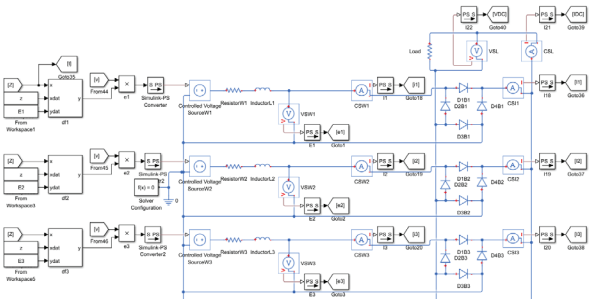

Figure 7: *Part of the harvester equivalent circuit model*

To convert the voltage from alternating to a direct one, we took 17 Greatz bridges, which were connected to the winding terminals. The Greatz bridges were constructed with four diodes, and had default Simscape values of 0.3 Ω. One AC Greatz bridge terminal was then connected directly to the winding terminal and the second terminal was connected to the winding over star/common point connection, which connected all windings together as presented in Fig. 7.

All Greatz bridge DC positive terminals were connected in parallel to create a positive DC link, and negative terminals were connected to the negative DC link. Both DC links were connected with the resistor, which presented the harvester`s load.

The mechanical behaviour of the mover was simulated with the mathematical model, which calculated the velocity of the mover with Eq (4) from the available kinetic energy. To obtain the available kinetic energy at a certain position, the spent energy (Wu) was subtracted, from the constant potential energy (Wp) of 0.5 m, as the law of energy conservation dictates,

$$v = \sqrt{\frac{2 \cdot W_{\mathrm{p}} - W_{\mathrm{u}}}{m + \frac{I}{r_{\mathrm{base}}}}} \tag{4.1}$$

where the spent energy in the system presented the sum of all electrical elements, losses and used energy by load, calculated with the Joule–Lenz law. With the prospect of running one simulation model, we used 0 mechanical inertia for translational movers, as the rest of the equation still holds true.

5 CLOSED LOOP DC LINK VOLTAGE

Fig. 8 shows the harvester's equivalent circuit model DC voltages at 10 Ω load, with the energy conservation law in place. If we compare the open circuit calculated DC voltages, where the movers displaced with constant velocity and amplitudes stayed in the bend, we can see voltage decline comprehensively with the mover's displacement over time, as a result of the velocity decrease.

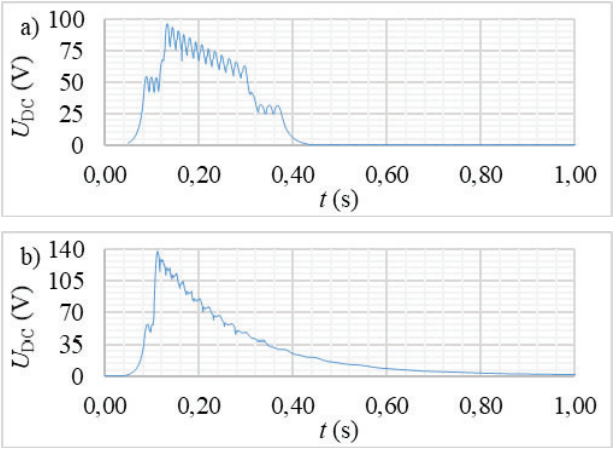

To be continued

Continuation

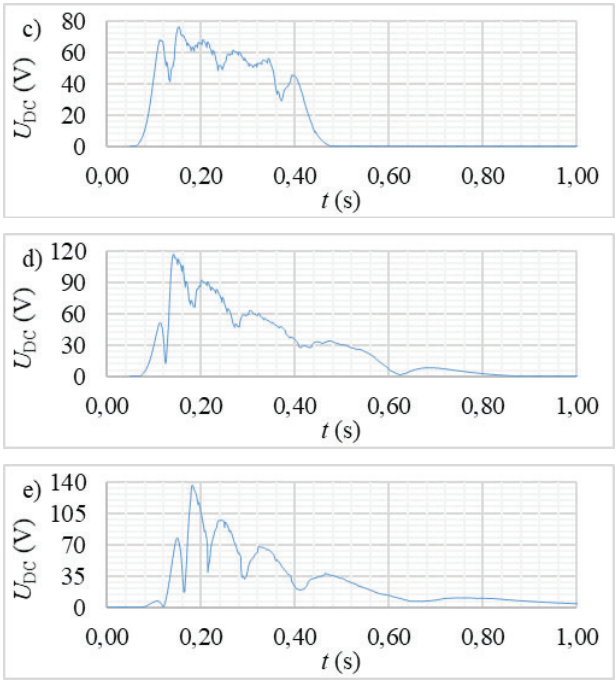

Figure 8: *Equivalent circuit direct voltage at 10 Ω load with alternating wound windings: a) Model A, b) Model B, c) Model C, d) Model D, e) Model E*

In Figs. 8 b), d) and e), where models B, D and E were simulated, we can see that the voltage converged slowly towards 0, until all the kinetic energy was transformed into electrical energy. On the other hand, in Figs. 8 a) and c), the voltage hit 0 steeply at 0.44 and 0.48 s. This can be explained with the velocity, as the movers were still travelling through the tube with high velocities of 1.79 and 1.68 m/s, and the magnetic field displaced too far from the windings to induce voltage, thus induction stopped.

6 KINETIC ENERGY UTILISATION AND ELECTRICAL EFFICIENCY

The goal of all harvesting machines is to extract the highest possible amount of energy. Extraction of energy was, in our case, determined predominantly by the induced voltage and current path resistance. As the winding's geometry and number of turns were fixed, this could be achieved by altering the circuit resistance with load, therefore, we extended the load range from 1 to 15 Ω.

We calculated the percentage of the extracted kinetic energy from the total available energy at the end of the simulation, with 1 Ω increments of loads, as shown in Fig. 9. With increasing load, as Ohms law dictates, current and generated power decreased. Although, too low power generation meant that the mover displaced out of the winding`s induction reach and part of the kinetic energy was not transformed. This is best presented with the mover`s end velocity v' (Fig. 10), which was taken either after displacement of 1.2 m or after 10 s of simulation. Figs. 9

and 10 show clearly, that the load ranges at which full kinetic energy can be extracted differed in all models.

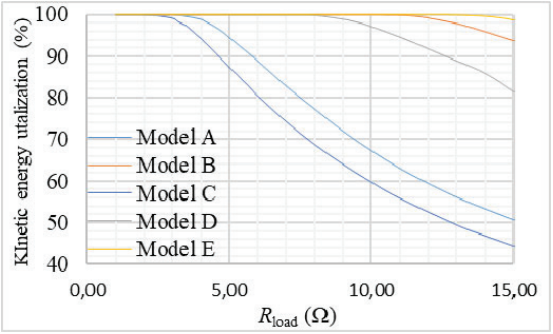

***Figure 9**: Mover`s kinetic energy utilisation*

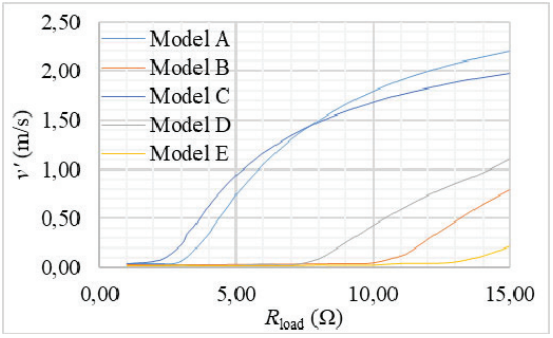

***Figure 8:** Mover velocity at the end of the simulation*

Models A and C, with the lowest induction velocity, had the smallest load ranges of 3 and 2 Ω respectively, of 100% kinetic energy utilisation. Models B and E with higher induced voltages had a wider range of load, which ended at 10 Ω in the case of model B and 14 Ω for model E. The mover in model D ran out of kinetic energy at 8 Ω load. The maximum load coincided inherently with the induced voltage, where models with a higher induced voltage had a wider range of load. This can be explained best with the translational displacing movers (Model A and B curves), that had the same winding resistance and different induced voltages. As the amount of power over time - energy was finite, we could generate a high power output over a short time with low resistance, or a lower power output with a higher resistance over a longer period of time/displacement. However, if the power output would be too low, the mover and magnetic field with it would displace too far away from the windings, so that induction could take place and leftover kinetic energy would go to waste, hence effecting the harvester`s yield.

Moreover, to improve the yield we needed to look from the efficiency perspective as well, as the lost energy from a circuit lowers the harvester`s output, even if all kinetic energy is transformed. Therefore, we calculated the electrical efficiencies in our load range for all models, which we obtained from the ratio between the energy lost on all elements of a circuit and energy consumed by the load. Models (A, B and C) with lower windings` resistances had a much higher electrical efficiency, as did the models (D and E) with higher resistance, as shown in Fig.

associated with lower energy losses in a circuit, as a consequence of smaller resistances of the windings, lower currents and higher energy consumption by the load with increase of load resistance.

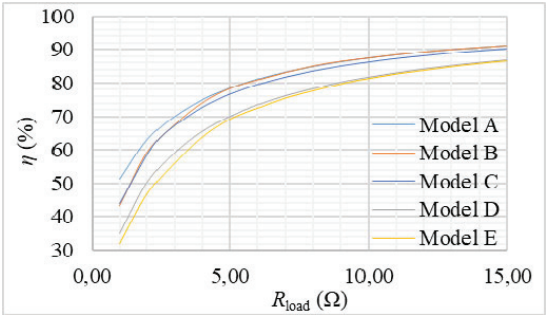

Figure 9: *Equivalent circuit electrical efficiency at a load range from 1 to 15 Ω.*

7 HARVESTER YIELD

As the main feature of energy harvesters is to harness the maximal amount of energy,to transform it into useful electrical energy is as important as the harvesting/extraction itself. When thinking about classical rotational generators, higher efficiency means better transformation of energy. However, in our case, we needed to take into account both efficiency and utilisation, as both affect a harvester`s yield. As the electrical efficiency is increasing, one would suspect that the highest yield would be at the biggest load, at which all kinetic energy is still utilised.

With the prospect of determining the best solution from the chosen designs, our objective was to find the highest yield point of each design to compare them to each other. For this reason, we ran simulations with different resistive loads at the same kinetic energy input for all presented models, trying to find a balance between losses and gains through utilisation of the whole generator length.

Energy yield was, therefore, determined with the ratio between kinetic energy on disposal and the energy used by the load.

$$yield = \frac{W_{\text{load}}}{W_{\text{k}}} \cdot 100 \tag{7.1}$$

To determine the highest yield point and at which load it occurs precisely, we calculated the yields with increments of 0.1 Ω, moving away from the previously obtained highest value of yield for ±1 Ω.

As **Napaka! Vira sklicevanja ni bilo mogoče najti.** shows, the maximum yield points were slightly pushed into higher loads as 0 end velocities were occurring. Model A, with a translational solid PM mover maximum yield was, at 4.5 Ω load, 74.52 %. The harvester with rolling spherical PM mover had 5.79 % lower maximum yield at 4 Ω. Model D, with the rolling cylindrical PM, had the highest yield of 79.69 % at 9.6 Ω. Harvesters B and E were the only ones which were operating above 80% yield already at 6 and 9.5 Ω, respectively. Model E had

reached a yield of 85,58 % at 14.7 Ω, and the absolute highest yield of 88,76 % was achieved by the composited mover made from PM and the steel plate, at 11.8 Ω.

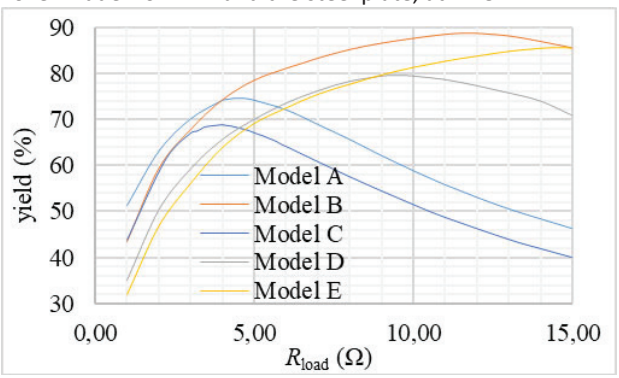

Figure 10: Equivalent circuit yield at load range from 1 to 15 Ω

For harvesters B and E we extended the load further, so that we could determine the range of the load, where both harvesters would yield more than 80 %. The B model`s last load over 80 % was at 18 Ω, where, for models E, it was at 20.4 Ω, which could be considered advantages, as loads could vary more than 5 Ω and the harvesters would still have reasonably good yields.

8 CONCLUSIONS

Hoping to create feasible and simple designs of an electromagnetic harvester, five proposed geometries were analysed, to determine the design with the highest yield.

Firstly, the magnetic flux waveforms and inductivity were calculated with the magnetostatic FEM in ANSYS. The same mass was used for all movers, although the shapes and displacement methods varied. Two movers were displacing translationally, and the other three were rolling throughthe stator, whereby one mover was forced into a higher angular velocity by spindles added on the sides of the mover. As a result of the different movers` geometries the windings had to be adjusted, although the windings` cross-sections stayed identical. From the magnetic flux waveforms, open circuit induced voltages were calculated at a constant centre of mass velocity, where the velocities were derived from kinetic energy, which was determined with the potential energy of 0.5 m.

Two winding configurations were calculated to find the highest induced voltage winding. The first configuration had all windings wound in the same direction and connected into a star connection. In the second winding configuration, the windings were wound in alternating directions, which turned out to be better configurations in all models, due to the higher induced voltages` potential differences.

An equivalent circuit model was constructed in Simulink and dynamic of harvester was simulated to conduct further evaluations. The mathematical part of the model calculated the velocity of the mover as it progressed through harvester, from the available kinetic energy, which was determined from the initial mover`s energy and electrical losses that accumulated over the time of displacement. The physical part, modelled with Simscape, presented the

windings, converter and load. The windings were modelled with a resistor, an inductor and a voltage source, which was driven by the magnetic flux gradient calculated in ANSYS and the velocity from the mathematical model. The converter part was modelled with four diodes in a Greatz bridge arrangement and converted windings AC to DC. The DC terminals of the converters were connected in parallel to establish positive and negative DC links. The DC links were connected with an ohmic load.

To determine the highest yield for every design, an array of simulations was conducted with loads from 1 to 15 Ω. As the results show, every harvester had a different optimal point of yield, as well as the highest yield itself. Models with higher induced voltages tended to have better yields, up to 85 %, compared to ones with lower induced voltages, regardless of their inner resistance and inductance. With higher voltages, as load resistance increased, more power could be shifted towards the load, as circuit losses decreased and efficiency improved, when still being able to convert all kinetic energy into electrical energy. Although as it turned out, maximum points of yield did not occur in a range of loads where all kinetic energy was spent, but slightly after, where a small part of the kinetic energy was still left in the mover.

Moreover, the design with the cylindrical translational mover with the concentrated magnetic flux pole and a rolling mover on spindles, which had the highest induced voltages, were able to operate over 80 % of yield at a high range of load, which could prove to be beneficial for harvesters with variable load or variable inbound mover velocity.

References

[1] **M. A. Mueller**: *Electrical generators for direct drive wave energy converters*, IEE Proceedings - Generation, Transmission and Distribution, vol. 149, no. 4, pp. 446-456, July 2002. Available: https://digital-library.theiet.org/content/journals/10.1049/ip-gtd_20020394

[2] **R. Alamian, R. Shafaghat, S. Jalal Miri, N. Yazdanshenas, M. Shakeri**: *Evaluation of technologies for harvesting wave energy in the Caspian Sea*, Renewable and Sustainable Energy Reviews, Volume 32, 2014. Available: https://doi.org/10.1016/j.rser.2014.01.036

[3] **Y. Cui, Z. Liu:** *Effects of Solidity Ratio on Performance of OWC Impulse Turbine*. Advances in Mechanical Engineering. January 2015. Available: https://doi.org/10.1155/2014/121373

[4] **S. Hor, A. Tabesh and A. Zamani**: *Analytical model of an improved linear generator for seawave energy harvesting,* IET Conference on Renewable Power Generation (RPG 2011), 2011, pp. 1-4, Available: https://doi: 10.1049/cp.2011.0230

[5] **A. Pirisi, M. Mussetta, F. Grimaccia, D. Caputo, G. Gruosso and R. E. Zich:** *An innovative device for traffic energy harvesting*, 6th IET International Conference on Power Electronics, Machines and Drives (PEMD 2012), Bristol, 2012, pp. 1-6. , Available: https://doi: 10.1049/cp.2012.0337

[6] **H. Li, P. Pillay:** *A Methodology to Design Linear Generators for Energy Conversion of Ambient Vibrations*, *2008 IEEE Industry Applications Society Annual Meeting*, 2008, pp. 1-8, Available: https//doi: 10.1109/08IAS.2008.72

[7] **L. Huang, J. Liu, H. Yu, R. Qu, H. Chen, and H. Fang:** *Winding configuration and performance investigations of a tubular superconducting flux-switching linear generator*, IEEE Trans. Appl. Supercond., vol. 25, no. 3, 2015. Available: https://doi: 10.1109/TASC.2014.2382877

[8] **G. Bracco, E. Giorcelli, and C. Attaianese:** *Design and experiments of linear tubular generators for the Inertial Sea Wave Energy Converter*, 2011 IEEE Energy Conversion Congress and Exposition, 2011, pp. 3864-3871, Available: https://doi: 10.1109/ECCE.2011.6064294

[9] **J. Asama, M. R. Burkhardt, F. Davoodi and J. W. Burdick:** *Investigation of energy harvesting circuit using a capacitor-sourced buck converter for a tubular linear generator of a moball: A spherical wind-driven exploration robot*, 2015 IEEE Energy Conversion Congress and Exposition (ECCE), 2015, pp. 3167-3171, Available: https:// doi: 10.1109/ECCE.2015.7310104

[10] **M. R. Burkhardt, F. Davoodi, J. W. Burdick, and F. Davoudi:** *Energy harvesting analysis for Moball, A self-propelled mobile sensor platform capable of long duration operation in harsh terrains*, Proc. - IEEE Int. Conf. Robot. Autom., pp. 2665–2672, 2014. Available: https://doi: 10.1109/ICRA.2014.6907241

[11] **S. Wu, P. C. K. Luk, C. Li, X. Zhao and Z. Jiao:** *Investigation of an Electromagnetic Wearable Resonance Kinetic Energy Harvester With Ferrofluid*, IEEE Transactions on Magnetics, vol. 53, no. 9, pp. 1-6, Sept. 2017, Art no. 4600706, Available: https://doi: 10.1109/TMAG.2017.2714621

[12] **N. Fondevilla et al:** *Electromagnetic harvester device for scavenging ambient mechanical energy with slow, variable, and randomness nature*, 2011 International Conference on Power Engineering, Energy and Electrical Drives, 2011, pp. 1-5, Availbale: https://doi: 10.1109/PowerEng.2011.6036432

[13] **J. Asama, M. R. Burkhardt, F. Davoodi and J. W. Burdick:** *Design investigation of a coreless tubular linear generator for a Moball: A spherical exploration robot with wind-energy harvesting capability,* 2015 IEEE International Conference on Robotics and Automation (ICRA), 2015, pp. 244-251, Available: https//doi: 10.1109/ICRA.2015.7139007

[14] **B. J. Bowers and D. P. Arnold:** *Spherical, rolling magnet generators for passive energy harvesting from human motion*, J. Micromechanics Microengineering, vol. 19, no. 9, 2009. Available: https:// doi:10.1088/0960-1317/19/9/094008

[15] **J. Joos and O. Paul:** *Spherical magnetic energy harvester with three orthogonal coils*, 2015 IEEE SENSORS, 2015, pp. 1-4, Available: https://doi:10.1109/ICSENS.2015.7370662

[16] **C.R. Saha, T. O'Donnell, N. Wang, P. McCloskey:** E*lectromagnetic generator for harvesting energy from human motion*, Sensors and Actuators A: Physical, Volume 147, Issue 1, 2008, Pages 248-253, Available: https://doi.org/10.1016/j.sna.2008.03.008

[17] **F. Pranjić, P. Virtič:** *Determination of an Optimum Fictitious Air Gap and Rotor Disk Thickness for a Coreless AFPMM*, Tehnicki Vjesnik, Vol. 25(6):1731-1738, December 2018, Available: https://doi:10.17559/TV-20171109105213